# Precise measurements of the $\gamma$-ray intensities following the $\beta$ decay of $^{144}$Ce and $^{147}$Nd

K. Kolos,[1,*] N. D. Scielzo,[1] V. E. Iacob,[2] J. C. Hardy,[2] A. M. Hennessy,[3] D. E. M. Hoff,[1] M. A. Stoyer,[1] A. P. Tonchev,[1] M. Bencomo,[1] J. A. Clark,[4] B. Champine,[5] P. Copp,[4] D. Melconian,[2] E. B. Norman,[5] W.-J. Ong,[1] H.-I. Park,[2] D. Santiago-Gonzalez,[4] G. Savard,[4,6] A. J. Shaka,[3] and S. Zhu[4]

[1]*Nuclear and Chemical Sciences Division, Lawrence Livermore National Laboratory, Livermore, California 94551, USA*
[2]*Cyclotron Institute, Texas A&M University, College Station, Texas 77843, USA*
[3]*Department of Chemistry, University of California, Irvine, California 92697, USA*
[4]*Physics Division, Argonne National Laboratory, Argonne, Illinois 60439, USA*
[5]*Department of Nuclear Engineering, University of California, Berkeley, California 94720, USA*
[6]*Department of Physics, University of Chicago, Chicago, Illinois 60637, USA*

(Received 11 December 2023; revised 12 June 2024; accepted 12 July 2024; published 12 August 2024)

For many fission products, the $\gamma$ rays emitted following $\beta$ decay provide an easily detectable signature that can be used to identify their quantities and distributions in a sample. As a result, $\gamma$-ray spectroscopy is often exploited to study fission-product yields, provided sufficiently accurate information on the $\gamma$-ray intensities is available. In many cases, the uncertainties in the existing nuclear data are large enough that they compromise the precision achievable for modern experiments and applications. In this paper, we present high-precision results for the absolute $\gamma$-ray emission intensities for the most intense transitions in the $\beta$ decays of $^{144}$Ce and $^{147}$Nd. We measured these intensities to $\lesssim$1% accuracy by producing radiopure samples with fission-product beams at CARIBU and detecting the emitted radiation with a $4\pi\beta$ counter and a meticulously efficiency-calibrated high purity germanium detector at Texas A&M University.

DOI: 10.1103/PhysRevC.110.024307

## I. INTRODUCTION

Nuclear fission is a collective phenomenon in which a heavy nucleus splits into two (or more) lighter nuclei either spontaneously or following interaction with an incident particle or photon. The distribution of the resulting fission products was first observed with semiquantitative measurements in 1939 [1], shortly after the discovery of this process [2,3]. These fission-product yields (FPYs) serve as key observables for understanding fission.

Today, high-quality nuclear data on FPYs aid in obtaining a deeper understanding of the fission process and its influence on the production of heavy elements in the cosmos, as well as for interpreting reactor experiments that scrutinize the fundamental properties of the neutrino. Many nuclear-science applications, ranging from the production of radioisotopes for medical applications, to the monitoring of nuclear reactors, to nuclear-security missions in stockpile stewardship and nuclear forensics [4–6], also benefit from reliable FPY data.

In the science-based Stockpile Stewardship Program (SSP), detailed in Ref. [7], the fission chain-reaction yields following historical nuclear tests could be determined from the quantities of certain key long-lived fission products, such as $^{95}$Zr, $^{144}$Ce, and $^{147}$Nd, collected in the radioactive debris. Given the importance of the FPYs of these particular isotopes for nuclear-security applications, providing high-quality nuclear decay data has been a matter of much interest in recent years.

The most common way that FPYs are determined is through the detection of the characteristic $\gamma$ rays emitted following the $\beta$ decays of the resulting fission products. The interpretation of these types of experiments depends on a precise knowledge of the absolute intensities of the emitted $\gamma$ rays, with the uncertainty in the absolute intensity directly contributing to the uncertainty in the deduced FPY.

Over the past decade, experiments utilizing $\gamma$-ray spectroscopy have measured the long-lived (cumulative) FPYs in neutron-induced fission with high statistics and careful control of systematics effects [8–14], such that the limitations in the existing nuclear data are a significant contributor to the overall uncertainty of the results. In these experiments, the detection of the most intense $\gamma$ rays emitted in the decay of the long-lived fission products $^{95}$Zr, $^{144}$Ce, and $^{147}$Nd was used to determine the production of the $A = 95$, $A = 144$, and $A = 147$ mass-chain yields in a sample [7,8].

In this paper, we present results from a set of precision measurements of the $\gamma$-ray intensities from the decays of $^{144}$Ce and $^{147}$Nd, providing the nuclear data necessary to interpret modern FPY measurements. Here, we extend the approach demonstrated in Ref. [15] with $^{95}$Zr to the more complicated decays of $^{144}$Ce, and $^{147}$Nd.

While the fission-product $^{95}$Zr has a simple decay scheme and extensive studies have determined the $\gamma$-ray intensities to 0.5% precision [15,16], the situation for $^{144}$Ce and $^{147}$Nd is not based on such a solid footing. The relative $\gamma$-ray

*Contact author: kolos1@llnl.gov

 

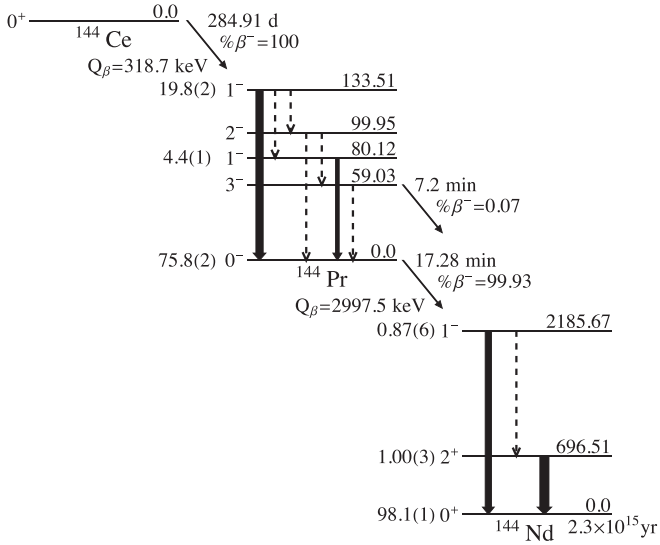


FIG. 1. Decay scheme for the chain from $^{144}$Ce to $^{144}$Pr to $^{144}$Nd, showing the main $\gamma$ rays in the decay with the lines not observed in this work as dashed lines (from NNDC). The values for the $\beta$-decay feeding are those from this work.

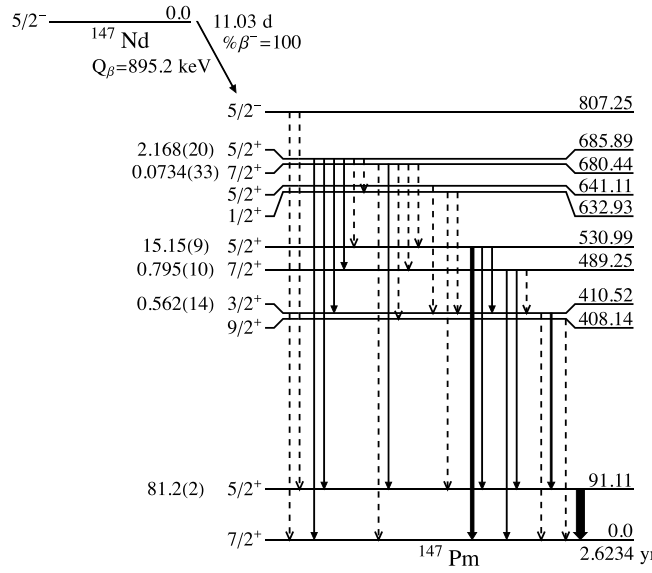


FIG. 2. Decay scheme for $^{147}$Nd decay to $^{147}$Pm (from NNDC) showing (solid) $\gamma$ rays observed (dashed) $\gamma$ rays not observed in this work. The $\beta$-decay feedings are those from this work.

intensities following the $\beta$ decay of $^{144}$Ce have been measured several times but there has been only a single absolute measurement, published nearly 50 years ago, which determined the intensity of the strongest transition, the 133.5-keV $\gamma$ ray, to a precision of 1.4% [17]. This result is used in the latest National Nuclear Data Center (NNDC) evaluation of the $\beta$ decay of $^{144}$Ce [18], which also adopts the relative values from Ref. [19] to establish the intensity of all the other $\gamma$ rays. Since the absolute $\gamma$-ray intensities for $^{144}$Ce decay are thus based on a single measurement [17], we set out to check this result and improve its precision. The relevant decay properties for $^{144}$Ce and its decay daughter $^{144}$Pr are shown in Fig. 1, where the $\beta$-decay feedings come from our work, and all other properties are from the latest evaluation [18]. Note that the ground-state–to–ground-state branch dominates in both cases, with $I_\beta = 76.0(2)\%$ and $98.1(1)\%$, respectively.

Until recently, the decay of $^{147}$Nd was even more ambiguous. In the Nuclear Data Sheet (NDS) evaluation [20] published in 2009, the intensity for the 531.0-keV $\gamma$ ray (the transition typically used to identify the presence of $^{147}$Nd in a sample) carried an uncertainty of 8%. This prompted us to mount an experiment to measure the intensity more precisely. In 2020 though, while our measurement was in progress, the situation changed significantly following a new measurement with 1% precision by Kellett *et al.* [21]. An updated NDS evaluation that incorporated that result followed shortly thereafter [22]. Our high-precision measurement now serves to further improve the precision and dependability of the absolute $\gamma$-ray intensities.

The relevant decay properties from the latest evaluation [22] for $^{147}$Nd are shown in Fig. 2, with $\beta$-decay feedings taken from our work. The $\beta$ decay of $^{147}$Nd primarily goes through the first excited state in $^{147}$Pm at 91.1 keV [with $I_\beta = 81.2(2)\%$] and to an excited state at 531.0 keV [$I_\beta = 15.15(9)\%$]; therefore, the most intense $\beta$-delayed $\gamma$-ray transitions are at 91.1 keV and 531.0 keV.

Our experimental method takes advantage of the mass-separated low-energy radioactive beams of fission products delivered by the CAlifornium Rare Isotope Breeder Upgrade (CARIBU) facility [23,24] at Argonne National Laboratory (ANL). The fission products are implanted in thin carbon foils, from which the emitted radiation emerges with minimal attenuation. These samples are then shipped to Texas A&M University (TAMU) in College Station, Texas, and inserted into a $4\pi$ gas proportional counter to detect $\beta$ particles. The $\gamma$ rays are detected with a meticulously efficiency-calibrated high purity germanium (HPGe) detector [25–27]. We determine the $\gamma$-ray intensities from a ratio of measured $\beta$-$\gamma$ coincidences to $\beta$ singles, after accounting for detection efficiencies and the fraction of the total detected $\beta$ particles attributed to the decay of the isotope of interest. The experimental procedure and detector efficiencies are described in detail in Ref. [15] where we demonstrated the approach by studying the $\beta$ decay of $^{95}$Zr.

## II. EXPERIMENTAL TECHNIQUE

### A. Source production

At CARIBU, products from the spontaneous fission of $^{252}$Cf are thermalized in a large helium-filled gas catcher [23] and extracted as a continuous low-energy ion beam from the nozzle of this device by a combination of gas flow and electric fields. The emerging ions are accelerated with a potential of 36 kV and sent through an isobar separator [28].

To produce the $^{144}$Ce sample, the mass slits of the isobar separator were set to select only ions with mass number to charge ratio $A/Q = 72$ corresponding to $A = 144$ fission products in the $2^+$ charge state. The isotopes in this mass chain with the highest yields are the short-lived $^{144}$Ba

[$T_{1/2} = 11.5(2)$ s] and $^{144}$La [$T_{1/2} = 40.8(4)$ s]. This beam of primarily $^{144}$Ba and $^{144}$La ions was then implanted into a 40 $\mu$g/cm$^2$ (200-nm) thick carbon foil. The decay of the accumulated isotopes built up a population of the long-lived $^{144}$Ce fission product. The integrated beam intensity delivered to the foil was determined every hour based on the accumulated number of 103.9-keV $\gamma$ rays from the decay of $^{144}$Ba and the 397.4-keV and 844.8-keV $\gamma$ rays from the decay of $^{144}$La detected with a HPGe detector continually monitoring the isotope-collection location. We used the time history of the $^{144}$Ba and $^{144}$La collection to gauge the number of $^{144}$Ce atoms accumulated in the foil. The accumulated $^{144}$Ce [$T_{1/2} = 284.91(5)$ d] quickly comes into secular equilibrium with its decay daughter $^{144}$Pr [$T_{1/2} = 17.28(5)$ min], with a small fraction proceeding by way of an isomeric state, $^{144m}$Pr [$T_{1/2} = 7.2(3)$ min]. Over a collection time period spanning 52 hours, the resulting $^{144}$Ce activity built up to about 840 Bq. By the time the sample was decay counted at TAMU over a year later, the $^{144}$Ce activity had decayed to 260 Bq.

The $^{147}$Nd sample was made in a similar way. In this case, the mass slits of the isobar separator were set to select only ions with $A/Q = 73.5$, corresponding to $A = 147$ fission products in the $2^+$ charge state. This beam was composed primarily of $^{147}$La [$T_{1/2} = 4.06(4)$ s] and $^{147}$Ce [$T_{1/2} = 56.4(10)$ s], which subsequently decayed to $^{147}$Pr [$T_{1/2} = 13.4(3)$ min], and then to $^{147}$Nd [$T_{1/2} = 11.03(3)$ d]. The average beam intensity over each hour was monitored by detecting the 117.7-keV $\gamma$ ray from the decay of $^{147}$La and the 580.0-keV and 701.1-keV $\gamma$ rays from the decay of $^{147}$Ce. Over a collection time of 64 hours (including the beam-off time), the activities deposited in the foil yielded about 1400 Bq of $^{147}$Nd. The decay of the daughter nucleus $^{147}$Pm [$T_{1/2} = 2.6234(2)$ y] contributes to the $\beta$-particle count rate, but produces no measurable $\gamma$ rays as the vast majority of decays (99.99%) populate the ground state of $^{147}$Sm directly. We used the time history of the collection to gauge the sample activity and to calculate the evolution of the resulting $^{147}$Nd-to-$^{147}$Pm activity ratio over the course of the experiment. This $^{147}$Nd sample was shipped to TAMU and arrived there within two days of the end of the collection.

### B. $\beta$-decay measurements

At TAMU, the samples were inserted into the center of the $4\pi$ gas proportional counter for $\beta$-particle detection. The $^{144}$Ce and $^{147}$Nd measurements were performed immediately after the $^{95}$Zr measurements described in [15], with the detection system in the same configuration. A brief description of this setup is provided here. More details about the optimization of the $4\pi$ gas proportional counter, including plateau measurements and the energy-threshold determination, can be found in Ref. [15].

The $\gamma$ rays emitted from the samples were detected with the meticulously efficiency-calibrated HPGe coaxial detector described in Refs. [25–27]. The source-detector distance was measured with a laser system [29] and determined to be 152.87(10) mm (as described in [15]). The photopeak efficiencies at this distance were obtained from the CYLTRAN [30] simulation. The $\beta$-$\gamma$ coincidence data were recorded event by event with a program written in the KmaxNT environment [31] and previously used in precise branching-ratio measurements (see, e.g., [32–34]). For $\beta$- and $\gamma$-ray signals arriving within 2 $\mu$s of each other, considered as "coincident", a master gate was generated and four parameters were recorded: the $\beta$ energy deposition in the $4\pi$ gas counter, the $\gamma$-ray energy deposition in the HPGe detector, the precise time difference between the detection of the two signals, and the absolute time of the coincidence. These data were collected in cycles for 54.93 s out of every 60 s.

The total numbers of $\beta$- and $\gamma$-ray singles were also stored with the KmaxNT system. The energy spectrum of the $\gamma$-ray singles was recorded independently with ORTEC EASY MCA handled by MAESTRO. The decay data for the $^{144}$Ce source were collected over a period of 6.5 days with the KmaxNT system, resulting in a total measurement time of $4.812 \times 10^5$ s (8760 cycles) with a source activity of about 260 Bq. The total measurement time for $\gamma$-ray singles, recorded with MAESTRO in parallel with the coincidence system, was just over 6.2 d (live time of $5.376 \times 10^5$ s).

The decay data for the $^{147}$Nd source, with an activity at the beginning of the measurement of 1160 Bq, were collected over a period of 4.7 d with the KmaxNT system, resulting in a total measurement time of $3.765 \times 10^5$ s (6855 cycles). The total measurement time for $\gamma$-ray singles, recorded with MAESTRO in parallel with the coincidence system, was about 5.4 d (live time of $4.697 \times 10^5$ s). The $\gamma$-ray singles background was collected for about 9.8 d ($8.425 \times 10^5$ s) between the source measurements. The $4\pi$-gas-counter background rate was 0.69(1) cps, and the background coincident count rate between the $4\pi$ gas counter and the HPGe detector was negligible.

## III. ANALYSIS

If one branch of a $\beta$-decaying nucleus populates an excited state in the daughter that $\gamma$-decays directly to its ground state without appreciable conversion or $\gamma$ feeding from higher excited states, then the intensity, $I_\gamma$, of that $\gamma$ ray relative to the total number of $\beta$ decays, is given by

$$I_\gamma = \frac{N_{\beta\gamma}}{N_\beta}\frac{\epsilon_\beta}{\epsilon_\gamma}\frac{\epsilon_\beta}{\epsilon_{\beta'}}, \tag{1}$$

where $N_{\beta\gamma}$ is the total number of $\beta$-$\gamma$ coincidences in the $\gamma$-ray peak of interest; $N_\beta$ is the total number of detected $\beta$ singles corresponding to the parent $\beta$ decay; $\epsilon_\gamma$ is the efficiency of the HPGe detector for detecting $\gamma$ rays of the relevant energy; $\epsilon_{\beta'}$ is the efficiency of the gas counter for detecting $\beta$s in the branch that populates the excited state; and $\epsilon_\beta$ is the average efficiency for detecting the $\beta$s from all decay branches. Note also that $\epsilon_{\beta'}$ can be determined experimentally via

$$\epsilon_{\beta'}(E_\gamma) = \frac{N_{\beta\gamma}}{N_\gamma}, \tag{2}$$

where $N_\gamma$ is the total number of singles $\gamma$ rays in the peak of interest.

In the nuclear decays being reported on here, the $\gamma$-ray transitions do indeed convert, which means that our gas

counter responded to conversion electrons as well as $\beta$-decay electrons. If $\epsilon_{\beta'}$ and $\epsilon_\beta$ were 100% this would have no impact on Eq. (1) since the conversion electrons would simply sum with already detected $\beta$-decay electrons. In fact, our $\beta$ efficiencies are 94% and above for all $\beta$ branches considered here, so conversion-electron contributions are suppressed by a factor of 20 or more. Nevertheless, we incorporate their effects by reinterpreting two of the terms in Eq. (1): We take $N_\beta$ to be the total number of counts—from $\beta$'s *and* conversion electrons—recorded in the gas counter; and, in determining $\epsilon_\beta$ we include in the detection efficiency the contribution from conversion electrons; and, in determining $\epsilon_{\beta'}$, we include the contribution from all conversion electrons and $\beta$s in cascades containing the relevant $\gamma$ in $N_{\beta\gamma}$. This slightly increases the effective value of $\epsilon_\beta$ but, for the strongest decay branches considered here, we compute the increase to be 1% or less. Thus $\epsilon_{\beta'}$ depends not only on the $\beta$ branches participating in a given cascade but also on the $\gamma$ transitions that contribute to the cascade. We label this corrected $\beta$ efficiency $\epsilon_{\beta'}(E_\gamma)$.

### A. $^{144}$Ce source

#### 1. $N_{\beta\gamma}$ determination

For each event, we recorded the time difference between the detected $\beta$- and $\gamma$-ray signals. The resultant time spectrum exhibited a "prompt" peak, corresponding to true coincidences, and a flat distribution on either side due to random coincidences. From this time spectrum we produced $\beta$-coincident $\gamma$-ray spectra free of random-coincidence events by first gating on the prompt peak and then subtracting random coincidences from gates, suitably normalized, on either side of the prompt peak. The resulting $\beta$-coincident $\gamma$-ray spectrum for $^{144}$Ce source is shown in Fig. 3(a).

To obtain the $\gamma$-ray peak areas, we used the fitting procedure described in Ref. [26], which is the same one used for the efficiency calibration of the HPGe detector. It employs a modified version of GF3, the least-squares peak-fitting program in the RADWARE series [35]. This method determines the number of counts in the peaks by integration of the spectrum above a well-defined background. The number of counts in the peaks at 80.1 and 133.5 keV were determined to be $9.18(14) \times 10^3$ and $59.69(26) \times 10^3$, respectively. We were also able to fit the peaks from the decay of the daughter nucleus $^{144}$Pr, which was present in the sample; the peaks at 696.5 and 2185.7 keV had $2.37(8) \times 10^3$ and $0.52(4) \times 10^3$ counts, respectively.

#### 2. Determination of $N_\beta$

A total of $1.2421 \times 10^8$ counts, accounting for background subtraction, were recorded in the $4\pi$ gas counter over the course of the measurement. The activities that contribute to this total must be carefully considered, since there is a non-negligible population of 7.2-min. $^{144m}$Pr, which decays predominantly by conversion electrons that would be detected in our $\beta$ detector. In fact, we find that we detect the decay of this isomer with 99.86(4)% efficiency.

We determined the fractional contributions to the total activity from the decays of $^{144}$Ce, $^{144}$Pr and $^{144m}$Pr using the Bateman equations, based on the time of the original

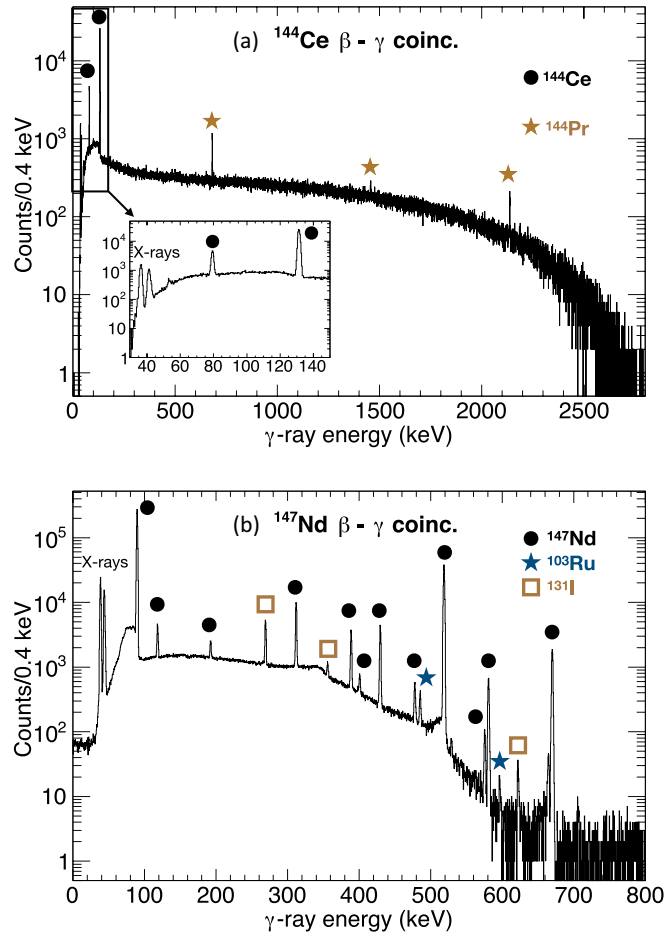


FIG. 3. The $\gamma$-ray spectrum measured in coincidence with $\beta$ particles for the $^{144}$Ce sample (top) and $^{147}$Nd sample (bottom). The peaks of interest are labeled by their $\beta$-decay parent. Note the broad $\beta$-particle background extending out to nearly 3 MeV in the $^{144}$Ce sample from the decay of $^{144}$Pr. This arises from $\beta$s that pass through the gas detector and then enter the HPGe detector, thus registering in both detectors.

source production (see Sec. II A), the results being 0.4969(2), 0.4969(2), and 0.0061(3), respectively. The uncertainty in this calculation is dominated by the uncertainty in the fraction of decays that populate the isomer as recorded in the most recent nuclear data evaluation [18]. From these activity fractions, we determined the relative contribution to the actual count rate in the $4\pi$ gas counter from each species by accounting for the small differences in detection efficiencies for the transitions (see Sec. III A 4). The resulting fraction of the total counts from $^{144}$Ce, $^{144}$Pr, and $^{144m}$Pr was 0.4928(23), 0.5009(23), and 0.0062(4), yielding total counts of $6.121(7) \times 10^7$, $6.222(7) \times 10^7$, and $0.078(4) \times 10^7$, respectively. The uncertainty in the fraction of total counts is dominated by the uncertainty in the $4\pi$ gas counter detection efficiency for the higher energy $\beta$ particles from the decay of $^{144}$Pr.

#### 3. $\gamma$-ray efficiencies

The HPGe detector setup was identical to that in Ref. [15]: The detector was surrounded by a cylindrical lead-plastic-

TABLE I. HPGe photopeak detector efficiencies for the $\gamma$ rays in the decays of $^{144}$Ce, $^{144}$Pr, and $^{147}$Nd obtained from the CYLTRAN simulation.

| $E_\gamma$ (keV) | $\epsilon_\gamma$ (%) |
|---|---|
| 80.1 | 0.9850(30) |
| 91.1 | 0.9765(29) |
| 120.5 | 0.9240(29) |
| 133.5 | 0.8942(27) |
| 196.6 | 0.7496(23) |
| 275.7 | 0.5996(18) |
| 319.4 | 0.5385(16) |
| 398.2 | 0.4565(18) |
| 439.9 | 0.4259(17) |
| 489.2 | 0.3930(15) |
| 531.0 | 0.3699(11) |
| 589.4 | 0.3431(15) |
| 594.8 | 0.3410(15) |
| 685.9 | 0.3082(9) |
| 696.5 | 0.3050(9) |
| 2185.7 | 0.1343(7) |

copper layered shield to attenuate the room background, and the source-to-detector distance was 152.87(10) mm. The photopeak efficiencies at this distance were obtained from the CYLTRAN simulation and are reported in Table I. These efficiencies were about 2.2% smaller than what would have applied at the calibration distance of 151.0 mm. For the most intense transitions, the simulated relative uncertainties are assigned a fractional uncertainty of 0.3%; for the other transitions, the efficiency was interpolated, and we assigned somewhat larger uncertainties, up to 0.5%.

#### *4. 4π gas counter efficiencies*

We obtained the $4\pi$ gas counter efficiencies for the decay transitions from a GEANT4 simulation of the apparatus. In our previous studies, we determined the detection threshold to be 0.7(1) keV, as described in Ref. [15]. To gain additional confidence in this threshold value, we compared our simulations to the values of $\epsilon_{\beta'}(E_\gamma)$ that were obtained from the current measurements via Eq. (2), the ratio of the $N_{\beta\gamma}$ coincidence counts to the singles counts, $N_\gamma$, for each individual $\gamma$ ray. To determine the $\gamma$-ray peak areas, we used the $\gamma$-ray singles spectrum after background subtraction and the same fitting procedure as used for the coincidence spectra. The coincidence and singles data were collected in parallel with two different data acquisition systems and had slightly different measurement times. Therefore, to directly compare these counts, we applied a decay correction to account for a $\lesssim 0.01\%$ and 0.1% difference in average activity expected for $^{144}$Ce and $^{147}$Nd, respectively, over the course of the measurement. For the strongest transitions in the decay of $^{144}$Ce and $^{147}$Nd, a comparison of $\epsilon_{\beta'}(E_\gamma)$ determined from our measurement and from the simulation with a 0.7-keV threshold is shown in Table II. As can be seen, the agreement across all the transitions is very good. With the accuracy of the simulations thus verified on individual transitions, we next

TABLE II. A comparison of $\epsilon_{\beta'}(E_\gamma)$ for transitions associated with $\gamma$-ray transitions in $^{144}$Ce and $^{147}$Nd determined from our measurement, $\epsilon_{\beta'}(E_\gamma)_{(\mathrm{exp})}$, compared with the simulation, $\epsilon_{\beta'}(E_\gamma)_{(\mathrm{calc})}$, that used a 0.7-keV threshold.

| Isotope | $E_\gamma$ | $E_{\beta_{max}}$ | $\epsilon_{\beta'}(E_\gamma)_{(\mathrm{exp})}$ | $\epsilon_{\beta'}(E_\gamma)_{(\mathrm{calc})}$ | $\frac{(\mathrm{exp})}{(\mathrm{calc})}$ |
|---|---|---|---|---|---|
| $^{144}$Ce | 80.1 | 238.7 | 96.0(28) | 95.52(31) | 1.005(30) |
| | 133.5 | 185.2 | 94.7(13) | 93.99(9) | 1.008(14) |
| $^{147}$Nd | 91.1 | 804.9 | 98.93(16) | 98.34(33) | 1.006(4) |
| | 319.4 | 485.5 | 98.56(58) | 98.84(18) | 0.997(6) |
| | 398.2 | 406.8 | 99.4(14) | 98.98(19) | 1.004(14) |
| | 531.0 | 364.9 | 97.28(4) | 97.07(48) | 1.002(5) |
| | 685.9 | 210.1 | 93.0(13) | 94.68(51) | 0.982(15) |

simulate the total efficiencies, $\epsilon_\beta$, for detecting the decays of $^{144}$Ce, $^{144}$Pr, $^{147}$Nd and $^{147}$Pm in the $4\pi$ gas counter. These were determined to be 96.7(4)%, 98.3(2)%, 99.1(2)%, and 95.1(1)%, respectively. The $^{147}$Nd efficiency is closer to 100% because a large fraction of the $\beta$ decays are accompanied by conversion-electron emission. The list of simulated efficiency ratios $\epsilon_\beta/\epsilon_{\beta'}(E_\gamma)$ for the observed transitions is presented in Table III. We determined the uncertainties on these values by varying the threshold by $\pm 1\sigma$ in the simulation.

These uncertainties also include an estimate of the effect of first-forbidden $\beta$ decay. We first simulated all of the transitions assuming an allowed shape. We then simulated, where applicable, the transitions as first-forbidden using a shape-correction fit to $^{210}$Bi data given by default in GEANT4. The difference between the two results for each transition was used as an estimate of the of the systematic error from the unknown shape of the $\beta$ spectrum, and was added in quadrature with

TABLE III. The $\beta$-particle detector-efficiency ratio for the $4\pi$ gas counter. The value of $E_{\beta_{\mathrm{max}}}$ corresponds to the highest energy $\beta$ particle that could be in coincidence with the $\gamma$ ray; in many cases, the associated $\beta$-energy spectrum is the result of more than one $\beta$ transition due to feeding from higher-lying states and includes any summing contributions from conversion electrons.

| Isotope | $E_\gamma$ (keV) | $E_{\beta_{max}}$ (keV) | $\epsilon_\beta/\epsilon_{\beta'}(E_\gamma)$ |
|---|---|---|---|
| $^{144}$Ce | 80.1 | 238.7 | 1.013(3) |
| | 133.5 | 185.2 | 1.037(2) |
| $^{144}$Pr | 696.5 | 2301.0 | 0.992(3) |
| | 2185.7 | 811.8 | 0.991(4) |
| $^{147}$Nd | 91.1 | 804.9 | 1.006(4) |
| | 120.5 | 364.9 | 1.001(4) |
| | 196.6 | 210.1 | 1.015(7) |
| | 275.7 | 210.1 | 1.009(4) |
| | 319.4 | 485.5 | 0.999(3) |
| | 398.2 | 406.8 | 1.001(3) |
| | 439.9 | 364.9 | 1.000(3) |
| | 489.2 | 406.8 | 1.022(4) |
| | 531.0 | 364.9 | 1.020(5) |
| | 589.4 | 215.6 | 1.009(14) |
| | 594.8 | 210.1 | 1.009(4) |
| | 685.9 | 210.1 | 1.045(7) |

TABLE IV. The $\gamma$-ray intensities (in %) obtained in this study compared with the most recent NNDC evaluation [18].

| Isotope | $E_\gamma$ | $I_\gamma$(this work) | $I_\gamma$(NNDC) |
|---|---|---|---|
| $^{144}$Ce | 80.1 | 1.538(27) | 1.364(58) |
| | 133.5 | 11.22(9) | 11.09(16) |
| $^{144}$Pr | 696.5 | 1.248(44) | 1.342(12) |
| | 2185.7 | 0.622(45) | 0.694(15) |

the other uncertainties. The values of $\epsilon_\beta$ and $\epsilon_{\beta'}(E_\gamma)$ are highly correlated, but to be conservative in estimating the total uncertainty, we treated them independently and added their uncertainties in quadrature.

#### 5. Absolute γ-ray intensities and β branching ratios

Using Eq. (1), we determined $I_\gamma$ for the 80.1- and 133.5-keV $\gamma$-ray transitions following the decay of $^{144}$Ce, and the 696.5 and 2185.7-keV $\gamma$-ray transitions following the decay of $^{144}$Pr. The results for the intensities are listed in Table IV, with the contributions to their fractional uncertainties being given in Table V. Our result for the 133.5-keV transition in the decay of $^{144}$Ce agrees with, and is more precise than, the NNDC evaluated value. However, there is a significant difference of 0.17(6)% between our result and the evaluation for the 80.1-keV transition. We note, though, that the measured intensity of the 80.1-keV transition relative to the 133.5-keV transition varies by up to 0.3% in previous published studies [19,36], easily encompassing our result; also, the publication giving the most precise determination of the 133.5-keV $\gamma$-ray intensity [17] did not provide a value for the 80.1-keV transition at all. For the two transitions from the decay of $^{144}$Pr, our results, although less precise, are consistent with the NNDC values within two standard deviations. With the factor of 2 improvement in precision of the $\gamma$-ray intensities associated with the decay $^{144}$Ce, we can provide updated $\beta$ branching ratios, including conversion electrons and feeding, for the decays of $^{144}$Ce and $^{144}$Pr. These appear in Table VI where it can be seen that the agreement with NNDC values is excellent.

### B. $^{147}$Nd source

#### 1. $N_{\beta\gamma}$ determination

The $\beta$-$\gamma$ coincidence spectrum obtained from the $^{147}$Nd source is shown in Fig. 3(b). We were able to determine the number of counts for 12 peaks, with the weakest one having

TABLE V. The contributions to the fractional uncertainty in $\gamma$-ray intensities following decays of $^{144}$Ce and $^{144}$Pr.

| $E_\gamma$ | 80.1 keV | 133.5 keV | 696.5 keV | 2185.7 keV |
|---|---|---|---|---|
| $N_{\beta\gamma}$ | 0.0156 | 0.0044 | 0.0350 | 0.0712 |
| $N_\beta$ | 0.0009 | 0.0009 | 0.0009 | 0.0009 |
| $\epsilon_\gamma$ | 0.0030 | 0.0030 | 0.0030 | 0.0050 |
| $\epsilon_\beta/\epsilon_{\beta'}(E_\gamma)$ | 0.0080 | 0.0060 | 0.0030 | 0.0040 |
| Total (%) | 1.75 | 0.80 | 3.53 | 7.17 |

TABLE VI. The $\beta$ branching ratios (in %) obtained in this study and compared with the most recent NNDC evaluation [18]. The ground-state feeding was calculated from 100 (summed $\beta$ feeding to other levels).

| Parent | Daughter level | $I_\beta$(this work) | $I_\beta$(NNDC) |
|---|---|---|---|
| $^{144}$Ce | 133.5 | 19.8(2) | 19.6(4) |
| | 80.12 | 4.2(1) | 3.9(2) |
| | 0 | 76.0(2) | 76.5(5) |
| $^{144}$Pr | 2185.7 | 0.87(6) | 1.05(4) |
| | 696.5 | 1.00(3) | 1.04(2) |
| | 0 | 98.1(1) | 97.9(4) |

an absolute intensity of only about 0.03%. The number of counts in the peaks at 91.1 and 531.0 keV were determined to be $1.215(16) \times 10^6$ and $2.046(4) \times 10^5$, respectively. For the 91.1-keV transition, the uncertainty is dominated by difficulties in characterizing the background on the left side of the peak that was caused by the scattering of these low-energy $\gamma$ rays from the copper housing on the $4\pi$ gas counter.

#### 2. Determination of $N_\beta$

A total of $4.3791 \times 10^8$ counts were recorded in the $4\pi$ gas counter over the course of the measurement. The coincidence $\beta$-$\gamma$ spectrum in Fig. 3(b) reveals the presence of small amounts of $^{131}$I and $^{103}$Ru in the sample, most likely from molecular contaminants in the original beam from CARIBU. These impurities contribute to the total number of $\beta$ particles detected in the $4\pi$ gas counter. We used the counts in the peaks at 364.3 keV and 497.2 keV, which have known absolute intensities [37,38] in the decays of $^{131}$I and $^{103}$Ru, respectively, to calculate the activity of these isotopes at the time of the measurement. Together the contributions from the two isotopes to the $\beta$ singles was estimated to be 0.2% of the total. The total number of $\beta$-particle counts from $^{147}$Nd and $^{147}$Pm after subtraction of background and isotopic contaminants was determined to be $4.3662(6) \times 10^8$.

To obtain the value of $N_\beta$ specifically for $^{147}$Nd, we also had to subtract the contribution from the grow-in of its daughter $^{147}$Pm. The $^{147}$Pm activity was calculated based on the time dependence of the implantation at CARIBU and the Bateman equations. Over the time window when the coincidence data were collected, the average $^{147}$Nd and $^{147}$Pm activities were determined to be 0.9939(1) and 0.0061(1) of the total, respectively. After accounting for the different $\beta$-particle detection efficiencies for the two isotopes [$\epsilon_{\rm Nd}/\epsilon_{\rm Pm} = 1.042(2)$], the resulting fractional contributions were 0.9942(1) and 0.0058(1). Expressed as $\beta$ counts, the results for $^{147}$Nd and $^{147}$Pm are $4.3407(7) \times 10^8$ and $2.546(44) \times 10^6$, respectively.

#### 3. Absolute γ-ray intensities

We determined the $\gamma$-ray intensities, $I_\gamma$, for the decay of $^{147}$Nd, obtaining a relative precision of 0.64–1.42 % for the transitions with absolute intensities greater than 0.3%. In Table VII, the complete list of the $\gamma$-ray intensities we obtained is compared to the values listed in the most recent evaluation [22]. In most cases, our intensities are more precise than the

TABLE VII. The $\gamma$-ray intensities (in %) following the decay of $^{147}$Nd obtained in this study and compared with the NNDC evaluation [22] from 2022.

| $E_\gamma$ | $I_\gamma$(this work) | $I_\gamma$(NNDC) |
|---|---|---|
| 91.1 | 28.88(41) | 28.95(50) |
| 120.5 | 0.378(5) | 0.369(5) |
| 196.6 | 0.175(6) | 0.181(4) |
| 275.7 | 0.777(9) | 0.791(16) |
| 319.4 | 1.915(13) | 1.967(25) |
| 398.2 | 0.841(9) | 0.867(13) |
| 439.9 | 1.188(11) | 1.203(16) |
| 489.2 | 0.139(4) | 0.142(5) |
| 531.0 | 13.02(8) | 13.11(13) |
| 589.4 | 0.034(3) | 0.039(1) |
| 594.8 | 0.253(5) | 0.243(4) |
| 685.9 | 0.815(10) | 0.823(17) |

ones appearing in the two evaluations; in all cases, they agree with them both within the given uncertainties.

The contributions to the uncertainties in the $I_\gamma$ results for the strongest $\gamma$ rays are given in Table VIII. For most transitions, the main component of the uncertainty comes from the determination of the number of counts in the $\gamma$-ray peaks in the $\beta$-$\gamma$ spectrum ($N_{\beta_\gamma}$). The uncertainty in the peak area is not just a matter of counting statistics—it includes the systematic uncertainty associated with the background subtraction. In particular, the counts in the 91-keV peak would be sufficient for a 0.1% statistical precision; however, the background under this peak is difficult to determine because scattering of these $\gamma$ rays from the $4\pi$ gas counter leads to a low-energy shoulder that has a shape that is difficult to constrain. Even with this limitation, we were able to obtain the $\gamma$-ray intensity of that transition to better than 1.5% precision.

To determine the $\beta$-decay branching ratios, $I_\beta$, for $^{147}$Nd, we include the contribution from conversion electrons, and subtract any $\gamma$-ray feeding that populates the state of interest. For this analysis we used the updated level scheme from the most recent NNDC evaluation [22]. The $\gamma$-ray feeding transitions, intensities of $\gamma$-ray transitions that we did not see in this experiment, and the conversion coefficients were also taken from Ref. [22]. The results of our calculated $\beta$ branching ratios are presented in Table IX.

We have chosen to present our findings in the same manner as the most recent NNDC evaluation by forcing the intensities

TABLE VIII. The contributions to the fractional uncertainty in intensities for the strongest $\gamma$ rays emitted following the decay of $^{147}$Nd.

| $E_\gamma$(keV) | 91.1 | 319.4 | 398.2 | 531.0 | 685.9 |
|---|---|---|---|---|---|
| $N_{\beta_\gamma}$ | 0.0133 | 0.0057 | 0.0096 | 0.0022 | 0.0098 |
| $N_\beta$ | 0.0002 | 0.0002 | 0.0002 | 0.0002 | 0.0002 |
| $\epsilon_\gamma$ | 0.0030 | 0.0030 | 0.0030 | 0.0030 | 0.0030 |
| $\epsilon_\beta/\epsilon_{\beta'}(E_\gamma)$ | 0.0037 | 0.0027 | 0.0034 | 0.0053 | 0.0069 |
| Total (%) | 1.42 | 0.70 | 1.08 | 0.62 | 1.17 |

TABLE IX. The $\beta$ branching ratios (in %) in the decay of $^{147}$Nd obtained in this study and compared with the most recent NNDC evaluation [22]. The $I_\beta$ for the level at 91.1 keV was calculated from 100% (summed $\beta$ feeding to other levels).

| Level energy | $I_\beta$(this work) | $I_\beta$(NNDC) |
|---|---|---|
| 807.25 | – | 0.0058(13) |
| 685.89 | 2.17(2) | 2.19(4) |
| 680.44 | 0.0734(33) | 0.0782(18) |
| 641.11 | – | 0.0051(5) |
| 632.93 | – | <0.006 |
| 530.998 | 15.15(9) | 15.25(21) |
| 489.255 | 0.795(10) | 0.819(15) |
| 410.515 | 0.562(14) | 0.62(3) |
| 91.1 | 81.2(2) | 81.0(3) |
| 0.0 | – | <0.3 |

to add up to exactly 100%. Like the NNDC, we did this by fixing the feeding of the 91.1-keV level to the value found when subtracting the sum of all the other feedings from 100%. If, instead, we were to calculate the feeding directly, as done for the other levels, we would find a total feeding to the 91.1-keV level of 82.8(15)%, leading to a summed $\beta$-decay intensity to all states of 101.7(15)%. Similar results are found if the feedings are taken from the NNDC evaluation. We note that while conversion electrons play a minor role in the derivation of $I_\gamma$ for the 91.1-keV state, they play an out-sized role in the calculation of the $I_\beta$ feeding to that state since the 91.1-keV $\gamma$ ray is heavily converted.

## IV. CONCLUSIONS

We have precisely measured the $\gamma$-ray intensities following the $\beta$ decay of $^{144}$Ce and $^{147}$Nd. Radiopure samples of mass-separated short-lived $A = 144$ and $A = 147$ fission products were collected at the CARIBU facility on a thin carbon foil. Within a few hours, the short-lived activities decayed to the longer-lived species of interest. The samples were then shipped to TAMU, where we detected the emitted $\beta$ particles and $\gamma$ rays in coincidence with a $4\pi$ gas counter and a HPGe detector. The efficiency of the HPGe detector had been characterized in detail, and the response of the $4\pi$ gas counter to low-energy $\beta$ particles was thoroughly investigated through comparison of GEANT4 model results with data.

Our measurements with the CARIBU-made sample resulted in absolute $\gamma$-ray intensities with uncertainties of 0.8–3 % for the strongest transitions in $^{144}$Ce, 3–6 % for $^{144}$Pr, and 0.6–1.4 % for $^{147}$Nd. Our results are in good agreement with the latest NNDC evaluation for the transitions in $^{144}$Pr and for the 133.5-keV transition in $^{144}$Ce. We obtained a different result from the evaluation for the 80.1-keV transition but our result is the most precise measurement of the absolute $\gamma$-ray intensity for this transition to date. For the decay of $^{147}$Nd, our measured intensity of the 531-keV transition, the strongest one, agrees within $1\sigma$ with the most recent evaluation and is the most precise measurement of that intensity yet reported. The other $\gamma$-ray intensities for this decay generally improve the precisions quoted in previous evaluations.

The method described in this paper is well suited to precise $\beta$-decay measurements of other fission products of importance to stockpile stewardship, nuclear forensics and other applications. We have been carrying out multiple experiments addressing discrepancies in the long-lived fission-product decay data and will report on the results in future publications.

## ACKNOWLEDGMENTS

This work was performed under the auspices of the U.S. Department of Energy (DOE) by the Lawrence Livermore National Laboratory (LLNL) under Contracts No. DE-AC52-07NA27344, No. DE-AC02-06CH11357 (ANL), and No. DE-FG03-93ER40773 (TAMU), and the University of California under Contract No. DE-AC0376SF0098. This work was supported in part by the Laboratory Directed Research and Development (LDRD) program at LLNL under Project No. 15-ERD-015, by the U.S. DOE National Nuclear Security Administration through the Office of Nonproliferation Research and Development (NA-22) under the Funding Opportunity Announcement LAB 17-1763, through the Nuclear Science and Security Consortium under Grant No. DE-NA-0000979, and by the Department of Energy, National Nuclear Security Administration through the Center for Excellence in Nuclear Training And University-based Research (CENTAUR) under Award No. DE-NA0003841.

[1] W. Jentschke and F. Prankl, Naturwissenschaften **27**, 135 (1939).
[2] O. Hahn and F. Strassman, Naturwissenschaften **27**, 89 (1939).
[3] L. Meitner and O. Frisch, Nature **143**, 239 (1939).
[4] M. B. Chadwick, T. Kawano, D. W. Barr, M. R. Mac Innes, A. C. Kahler, T. Graves, H. Selby, C. J. Burns, W. C. Inkret, A. L. Keksis, J. P. Lestone, A. J. Sierk, and P. Talou, Nucl. Data Sheets **111**, 2923 (2010).
[5] J. Laurec, A. Adam, T. de Bruyne, E. Bauge, T. Granier, J. Aupiais, O. Bersillon, G. Le Petit, N. Authier, and P. Casoli, Nucl. Data Sheets **111**, 2965 (2010).
[6] M. Mac Innes, M. Chadwick, and T. Kawano, Nucl. Data Sheets **112**, 3135 (2010).
[7] H. D. Selby, M. R. M. Innes, D. W. Barr, A. L. Keksis, R. A. Meade, C. J. Burns, M. B. Chadwick, and T. C. Wallstrom, Nucl. Data Sheets **111**, 2891 (2010).
[8] M. E. Gooden, C. W. Arnold, J. A. Becker, C. Bhatia, M. Bhike, E. M. Bond, T. A. Bredeweg, B. Fallin, M. M. Fowler, C. R. Howell, J. H. Kelley, Krishichayan, R. Macri, G. Rusev, C. Ryan, S. A. Sheets, M. A. Stoyer, A. P. Tonchev, W. Tornow, D. J. Vieira *et al.*, Nucl. Data Sheets **131**, 319 (2016).
[9] C. Bhatia, B. Fallin, M. Gooden, C. Howell, J. Kelley, W. Tornow, C. Arnold, E. Bond, T. Bredeweg, M. Fowler, W. Moody, R. Rundberg, G. Rusev, D. Vieira, J. Wilhelmy, J. Becker, R. Macri, C. Ryan, S. Sheets, M. Stoyer *et al.*, Nucl. Instrum. Methods Phys. Res. A **757**, 7 (2014).
[10] C. Bhatia, B. F. Fallin, M. E. Gooden, C. R. Howell, J. H. Kelley, W. Tornow, C. W. Arnold, E. Bond, T. A. Bredeweg, M. M. Fowler, W. Moody, R. S. Rundberg, G. Y. Rusev, D. J. Vieira, J. B. Wilhelmy, J. A. Becker, R. Macri, C. Ryan, S. A. Sheets, M. A. Stoyer *et al.*, Phys. Rev. C **91**, 064604 (2015).
[11] M. Bhike, W. Tornow, Krishichayan, and A. P. Tonchev, Phys. Rev. C **95**, 024608 (2017).
[12] Krishichayan, M. Bhike, S. Finch, C. Howell, A. Tonchev, and W. Tornow, Nucl. Instrum. Methods Phys. Res. A **854**, 40 (2017).
[13] M. A. Stoyer, A. P. Tonchev, J. A. Silano, M. E. Gooden, J. B. Wilhelmy, W. Tornow, C. R. Howell, F. Krishichayan, and S. Finch, EPJ Web Conf. **232**, 03006 (2020).
[14] A. P. D. Ramirez, J. A. Silano, R. C. Malone, M. A. Stoyer, A. P. Tonchev, M. E. Gooden, J. B. Wilhelmy, S. W. Finch, C. R. Howell, Krishichayan, and W. Tornow, Phys. Rev. C **107**, 054608 (2023).
[15] K. Kolos, A. Hennessy, N. Scielzo, V. Iacob, J. Hardy, M. Stoyer, A. Tonchev, W.-J. Ong, M. Burkey, B. Champine, J. Clark, P. Copp, A. Gallant, E. Norman, R. Orford, H. Park, J. Rohrer, D. Santiago-Gonzalez, G. Savard, A. Shaka *et al.*, Nucl. Instrum. Methods Phys. Res. A **1000**, 165240 (2021).
[16] S. K. Basu, G. Mukherjee, and A. A. Sonzogni, Nucl. Data Sheets **111**, 2555 (2010).
[17] K. Debertin, U. Schötzig, K. F. Walz, and H. M. Weiss, Ann. Nucl. Energy **2**, 37 (1975).
[18] A. A. Sonzogni, Nucl. Data Sheets **93**, 599 (2001).
[19] J. Dalmasso, H. Maria, A. Hachem, and G. Ardisson, Nucl. Instrum. Methods Phys. Res. **221**, 564 (1984).
[20] N. Nica, Nucl. Data Sheets **110**, 749 (2009).
[21] M. Kellett, L. Vio, C. Bobin, L. Brondeau, M. Cardot-Martin, H. Isnard, D. Lacour, M.-C. Lépy, V. Lourenço, M. Marie, and C. Thiam, Appl. Radiat. Isot. **166**, 109349 (2020).
[22] N. Nica and B. Singh, Nucl. Data Sheets **181**, 1 (2022).
[23] G. Savard, S. Baker, C. Davids, A. F. Levand, E. F. Moore, R. C. Pardo, R. Vondrasek, B. J. Zabransky, and G. Zinkann, Nucl. Instrum. Methods Phys. Res. B **266**, 4086 (2008).
[24] G. Savard, A. F. Levand, and B. J. Zabransky, Nucl. Instrum. Methods Phys. Res. B **376**, 246 (2016).
[25] J. C. Hardy, V. E. Iacob, M. Sanchez-Vega, R. Effinger, P. Lipnik, V. E. Mayes, D. K. Willis, and R. G. Helmer, Appl. Radiat. Isot. **56**, 65 (2002).
[26] R. G. Helmer, J. C. Hardy, V. E. Iacob, M. Sanchez-Vega, R. G. Neilson, and J. Nelson, Nucl. Instrum. Methods Phys. Res.A **511**, 360 (2003).
[27] R. G. Helmer, N. Nica, J. C. Hardy, and V. E. Iacob, Appl. Radiat. Isot. **60**, 173 (2004).
[28] C. N. Davids and D. Peterson, Nucl. Instrum. Methods Phys. Res. B **266**, 4449 (2008).
[29] AcuityLaser, http://www.acuitylaser.com (2019).
[30] J. A. Halbleib and T. A. Mehlhorn, Nucl. Sci. Eng. **92**, 338 (1986).
[31] Sparrowcorp, http://www.sparrowcorp.com (2019), the previously published non-Java version of the code developed for Windows NT was used.
[32] H. I. Park, J. C. Hardy, V. E. Iacob, M. Bencomo, L. Chen, V. Horvat, N. Nica, B. T. Roeder, E. McCleskey, R. E. Tribble, and I. S. Towner, Phys. Rev. C **92**, 015502 (2015).
[33] M. Bencomo, J. C. Hardy, V. E. Iacob, H. I. Park, L. Chen, V. Horvat, N. Nica, B. T. Roeder, A. Saastamoinen, and I. S. Towner, Phys. Rev. C **100**, 015503 (2019).

[34] V. E. Iacob, J. C. Hardy, H. I. Park, M. Bencomo, L. Chen, V. Horvat, N. Nica, B. T. Roeder, A. Saastamoinen, and I. S. Towner, Phys. Rev. C **101**, 045501 (2020).
[35] D. C. Radford, https://radware.phy.ornl.gov (private communication) (2000).
[36] B. V. N. Rao and G. N. Rao, J. Phys. Soc. Jpn. **40**, 1 (1976).
[37] Y. Khazov, I. Mitropolsky, and A. Rodionov, Nucl. Data Sheets **107**, 2715 (2006).
[38] D. D. Frenne, Nucl. Data Sheets **110**, 2081 (2009).